Selective permeability of mouse blood-aqueous barrier as determined by ^{15}N-heavy isotope tracing and mass spectrometry

Pan Liu[a], Benjamin R. Thomson[a], Natalia Khalatyan[b], Liang Feng[c], Xiaorong Liu[c,1], Jeffrey N. Savas[b], Susan E. Quaggin[a], and Jing Jin[a,2]

[a]Division of Nephrology and Hypertension, Feinberg Cardiovascular and Renal Research Institute, Feinberg School of Medicine, Northwestern University, Chicago, IL 60611; [b]Department of Neurology, Feinberg School of Medicine, Northwestern University, Chicago, IL 60611; and [c]Department of Ophthalmology, Feinberg School of Medicine, Northwestern University, Chicago, IL 60611

Edited by David J. Calkins, Vanderbilt University Medical Center, Nashville, TN, and accepted by Editorial Board Member Jeremy Nathans July 24, 2018 (received for review May 8, 2018)

The blood-aqueous barrier plays a key role in regulating aqueous humor homeostasis by selectively restricting passage of proteins into the eye. The kinetics of aqueous flow are traditionally measured using artificial markers; however, these marker molecules do not address the barrier's selective permeability to plasma proteins. Here we applied stable isotope labeling of all serum proteins with nitrogen-15 (^{15}N) atoms. Following systemic injection of this "heavy" serum in mice, the ^{15}N-to-endogenous nitrogen-14 (^{14}N) ratio of each protein in aqueous was measured by mass spectrometry. By monitoring the kinetic changes in these ratios, we determined the permeability profiles of hundreds of serum proteins. Meanwhile, we subjected one of the eyes to neoangiogenic wound healing by inflicting injury to the corneal limbus and compared the ^{15}N proteomes between the normal eyes and the recovering eyes at 2 weeks after injury. In the injured eye, we detected markedly enhanced permeability to inhibitory complement regulator proteins, such as Cfh, Cfhr, Cfb, Cfi, Cfd, and Vtn. Many of the proteins in this group are implicated in age-related macular degeneration associated with leakage of the blood-retinal barrier due to inflammation. To rule out the possibility that the observed leakage was due simply to physical damage of the blood vessels, we separately created a neovascularization model using an alkali burn of the avascular cornea. In this latter model, elevated levels of Cfh and Cfb were evident. These findings suggest that ocular neovascularization is associated with enhanced permeability to serum complement regulators.

blood-aqueous barrier | blood-ocular barrier | proteomics | stable isotope labeling in mammals | complement system

Within the mammalian eye, the access of water and proteins from blood circulation to aqueous and vitreous is tightly controlled by complex blood-ocular barriers (1–3). These selective barriers prevent certain plasma proteins from entering the eye, an essential function to maintain ocular immune privilege (4, 5). Two major barriers of the eye have been studied extensively in health and disease: the blood-aqueous barrier (BAB), located in the anterior segment of the ciliary body, and the blood-retinal barrier (BRB), distributed widely across the posterior segment. Significant amounts of aqueous humor proteins are plasma-derived and are filtered mainly through the aqueous barrier, move across stroma of the ciliary body and the stroma of the iris, and then released into the aqueous of the anterior chamber (6–8).

Traditionally, permeability of the aqueous barrier is quantitatively measured using individual molecular tracers, such as fluorescein (9), horseradish peroxidase (10), radiolabeled albumin (11), and other protein or nonprotein molecules (8, 12). These tracers are used to identify changes in vascular permeability and to measure aqueous flow rate in human eye disease. Regarding the barrier's selectivity, it is generally believed that aqueous is not a simple ultrafiltrate of plasma; however, methods for qualitative measurement of the barrier's selectivity to individual plasma proteins are lacking, and the mechanisms underlying the selective permeability remain elusive. Neither the size of plasma proteins nor their charge state, or any other recognizable biophysical properties, determine the ability to cross the barrier (13). Furthermore, certain proteins are present in higher concentration in aqueous than in plasma (2), suggesting that they are actively transported and/or locally synthesized. Local synthesis in the eye produces many proteins also found in the plasma (14). While details about protein composition in aqueous (15) and in plasma are known, the extent of plasma proteins that are permitted to cross the BAB vs. those that are produced in the eye remains unclear.

To directly address this problem, we devised an approach using complete mouse serum—instead of a single protein—as a tracer to monitor the entry of individual proteins into aqueous. To accomplish this, the tracer serum proteins were all labeled

Significance

The aqueous fluid of the eye is composed of proteins from both blood circulation and ocular production. The main filter between the blood bed and the intraocular fluid is referred to as the blood-aqueous barrier. Here we devised an approach to address the selectivity of the barrier using nitrogen-15–labeled serum proteins as tracers. Following systemic injection of the labeled serum to normal nitrogen-14 mice, the labeled proteins subsequently entered the aqueous fluid and were measured by mass spectrometry. This new quantitative method captured the dynamic redistribution patterns of approximately 500 serum proteins entering normal eye and the eye recovering from injury. We discovered inhibitory complement proteins crossed the blood-ocular barrier of the wounded eye but not of the normal eye.

Author contributions: P.L. and J.J. designed research; P.L., B.R.T., N.K., and L.F. performed research; X.L., J.N.S., and S.E.Q. contributed new reagents/analytic tools; P.L., N.K., J.N.S., and J.J. analyzed data; and P.L. and J.J. wrote the paper.

The authors declare no conflict of interest.

This article is a PNAS Direct Submission. D.J.C. is a guest editor invited by the Editorial Board.

Data deposition: All raw spectrum data are available through the MassIVE database (https://massive.ucsd.edu/ProteoSAFe/static/massive.jsp) via ProteomeXchange identifier PXD010366.

[1]Present address: Department of Biology, University of Virginia, Charlottesville, VA 22904; and Department of Psychology, University of Virginia, Charlottesville, VA 22904.

[2]To whom correspondence should be addressed. Email: jing.jin@northwestern.edu.

This article contains supporting information online at www.pnas.org/lookup/suppl/doi:10.1073/pnas.1807982115/-/DCSupplemental.

Published online August 20, 2018.

with nitrogen-15 (^{15}N) atoms following a metabolic process known as stable isotope labeling of mammals (SILAM) (16). We then i.v.-injected this ^{15}N-labeled serum into normal nitrogen-14 (^{14}N) mice and collected aqueous humor and serum from the recipient mice. By running SILAM-directed mass spectrometry (MS), corresponding ^{15}N- and ^{14}N-containing proteins were individually identified based on their respective molecular mass, and the relative abundance of the heavy and light counterparts was measured. As such, the kinetics of hundreds of serum proteins entering the aqueous were determined.

Results

Workflow for Aqueous Proteomics in Conjunction with ^{15}N-Labeling of Mouse Serum. The key technical aspect of our study is the use of metabolically labeled whole serum as a tracer, followed by detection of individual aqueous proteins carrying ^{15}N atoms by liquid chromatography tandem mass spectrometry (LC-MS/MS) (Fig. 1). We used a SILAM protocol to label C57BL/6J mice by providing a single source of ^{15}N-labeled nitrogen in chow with the complete absence of ^{14}N. After 12 wk of a restrictive diet, the mice were significantly enriched with ^{15}N at each amino acid position. For this study, we collected ^{15}N-serum from these mice. Via a tail vein, we infused a bolus of the "heavy" ^{15}N-serum to normal ^{14}N mice of a isogenic strain and then collected aqueous and serum from the recipient mice.

The entire protein contents in each sample were analyzed as tryptic peptides by LC-MS/MS. Peptides and proteins were each assigned to either the donor serum or the recipient mice based on the match between the observed molecular weight to the theoretical mass of either ^{15}N- or ^{14}N-containing sequences, respectively. In each sample, the relative amounts of ^{15}N and ^{14}N peptides of the same sequence were calculated to derive the ratio of exogenous (^{15}N) to endogenous (^{14}N) abundance (*Methods* and *SI Appendix*, Fig. S1). The ratios at a specified time point of collection reflect the cumulative exchange by ^{15}N-labeled serum proteins that had entered aqueous from blood.

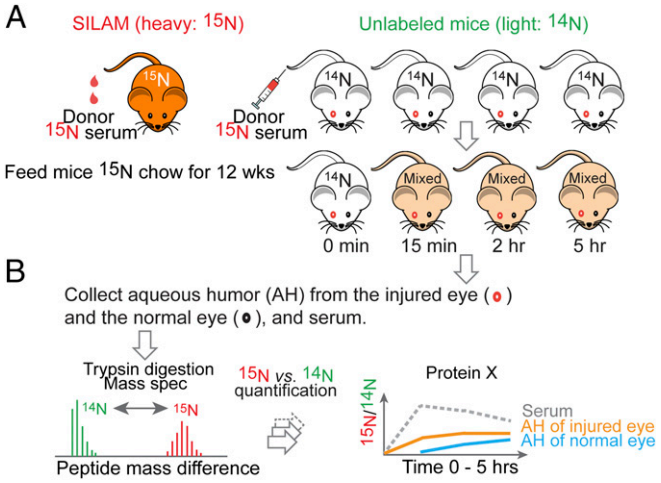

Fig. 1. Workflow for measuring kinetic entries of plasma proteins into aqueous using ^{15}N-labeled mouse serum as a tracer. (*A*) ^{15}N-labeled serum was collected from donor mice that were metabolically labeled with ^{15}N via SILAM. Then 300 μL of ^{15}N-labeled serum was injected into the tail vein of ^{14}N mice. Before receiving ^{15}N serum, these subject mice had been prepared with one of the two eyes injured, and then allowed to recover for 2 wk. Aqueous from each eye and serum samples were collected following a time course. (*B*) The aqueous contents of ^{15}N-labeled proteins were measured as ^{15}N/^{14}N ratios for individual proteins by LC-MS/MS.

Serum and Aqueous Distributions of ^{15}N-Labeled Proteins Show Selective Permeability of the BAB. Unlike the conventional SILAM-based approach that mixes ^{15}N lysate with those from the subject mice (17, 18), in the current application we injected ^{15}N-labeled serum to live animals to measure in vivo barrier-crossing kinetics. First, we compared three serum samples, collected from a ^{15}N-labeled mouse, an unlabeled mouse, and an unlabeled mouse 15 min after an injection of ^{15}N serum. The ^{15}N/^{14}N ratios were measured in peptides identified by MS. Fig. 2*A*, *Top* shows scatterplots of these ratios along the *x*-axis and the number of identified peptides for each protein along the *y*-axis. As expected, the vast majority of proteins identified from mice with "normal" serum (no injection) had a ^{15}N/^{14}N ratio of 0, whereas protein ratios from mice with proteins labeled with ^{15}N were uniformly high. In unlabeled mice that had received an injection of ^{15}N serum, the protein ratios showed intermediate values. The plotting patterns provide an important validation of this method of measuring the relative abundance of each ^{15}N-labeled protein using the corresponding ^{14}N-protein from the serum recipient mouse as the reference.

We applied the analysis of ^{15}N/^{14}N ratios to proteins extracted from the aqueous humor of normal mice that had received an i.v. bolus of ^{15}N serum. ^{15}N proteins could be sensitively detected as early as 15 min, suggesting the BAB-crossing activities as highly dynamic (Fig. 2*A*, *Middle*). If we arbitrarily set a ^{15}N/^{14}N ratio of 0.02 as the cutoff and focus only on proteins also detectable in serum, 14% of the proteins reached this ratio in the aqueous humor by 15 min. By 5 h, 55% individual proteins had a ^{15}N/^{14}N ratio >0.02, indicating time-dependent movements of serum proteins cross the BAB. It is important to note that numerous ^{15}N serum proteins did not cross the BAB despite the clear presence of them in aqueous with only ^{14}N contents. This indicates that either these proteins are produced directly by eye tissues or they enter the eye from blood very slowly.

To examine the difference between a normal eye and an eye recovering from injury, we used a wound-healing model with only one of the two eyes in each mouse inflicted with injury and then allowed it to recover for 2 wk. Overall, there were far more proteins in the injured eye than in the healthy eye (577 vs. 148 in Fig. 2*A*, *Bottom*), suggesting increased barrier permeability following injury and/or tissue repair. The Venn diagram in Fig. 2*B* illustrates proteins that were detected in aqueous under different conditions. For those aqueous proteins that had both ^{14}N and ^{15}N components detectable by MS, after combining all protein isoforms, we focused on 136 proteins and calculated their blood-to-aqueous redistribution kinetics (*SI Appendix*, Figs. S2 and S3).

Along with the ^{15}N/^{14}N ratio, to determine the steady-state amount of individual proteins, we relied on the MS algorithms for normalized spectral abundance factor (NSAF) and exponentially modified protein abundance index (emPAI) that are commonly used for "label-free" quantification (19, 20). *SI Appendix*, Fig. S4 shows that quantifications using ^{15}N-labeled vs. label-free algorithmic approaches achieved comparable results. Based on NSAF index values, we identified the most abundant aqueous proteins (*SI Appendix*, Table S1 and Dataset S1). These include proteins of known blood origin, such as many carrier proteins as well as those produced locally in the eye, such as the main structural protein of the lens crystallins (21); GSTs, antioxidant enzymes important for maintaining a reduced chemical environment (22, 23); and prostaglandin synthase produced by the ciliary body (24).

Time-Dependent Entry of Serum Proteins to Aqueous. We next plotted the changes in ^{15}N/^{14}N ratios for those proteins that reached substantial concentrations in aqueous (≥30% relative to the ratio for the same protein in serum) (*SI Appendix*, Fig. S5*A* and Dataset S1). ^{15}N albumin showed a gradual increase in the aqueous over time to a point that its ^{15}N/^{14}N ratio reached

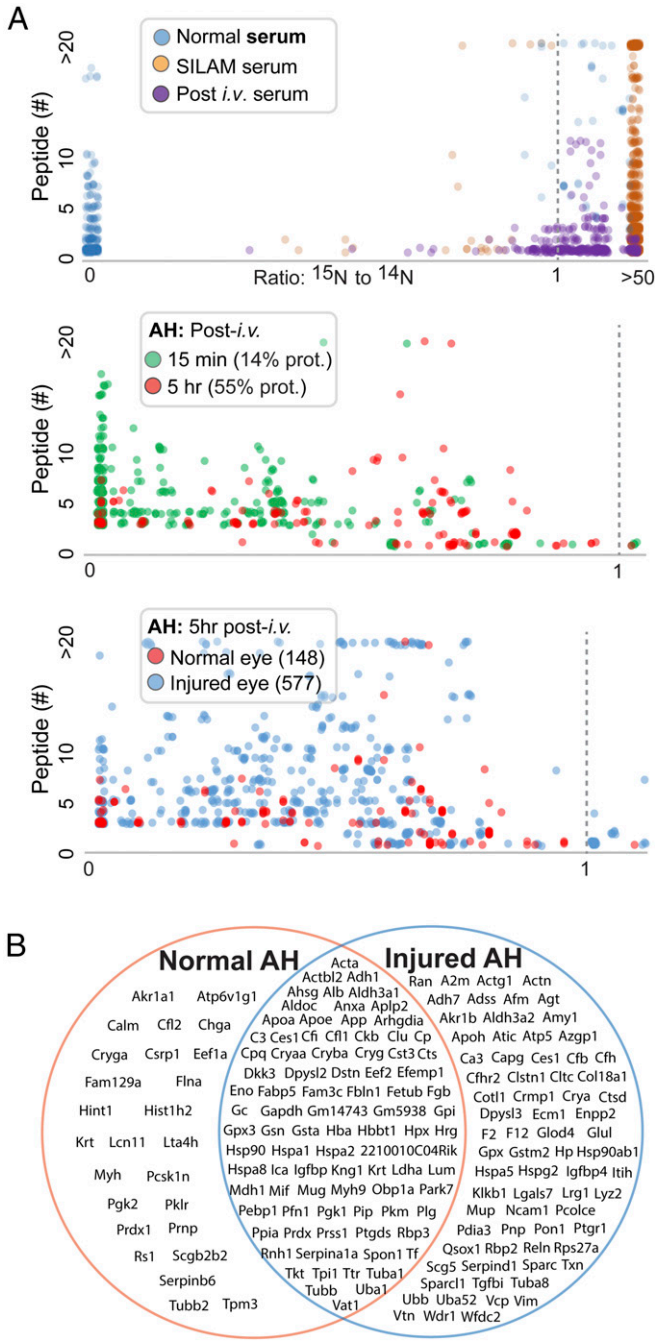

Fig. 2. Proteomic detection of aqueous proteins in conjunction with ^{15}N-labeled tracers. Each dot represents a protein. The heavy vs. light ratio for each protein is represented by the composite of all peptide ratios identified by MS that are assigned to the protein. (*A*, *Top*) Comparisons of sera collected from three different mouse groups: normal (^{14}N) mice, SILAM (^{15}N-labeled) mice, and normal mice at 15 min after receiving a bolus infusion of SILAM serum. The ^{15}N/^{14}N ratios are graphed between 0 and a "ceilinged" value at 50 to accommodate singleton proteins identified with only ^{14}N or ^{15}N peptides, respectively. (*A*, *Middle*) Comparison of aqueous humor (AH) collected at 15 min and 5 h. (*A*, *Bottom*) Comparison of the uninjured and injured eyes. (*B*) A total of seven eyes (three injured eyes and four uninjured eyes) were analyzed by MS, and aqueous humor proteins were detected. The three groups of proteins in the Venn diagram include proteins detected in all injured eyes but not in uninjured eyes, proteins detected in all uninjured eyes but not in injured eyes, and proteins detected in all seven eyes.

approximately 75% of its serum ratio after 5 h. We then sought to determine whether serum abundance of any individual protein generally correlated with its kinetics of aqueous entry, which would indicate a lack of protein-specific selectivity of the barrier. We plotted comparisons between NSAF indices for total serum abundance and aqueous ^{15}N/^{14}N ratios for BAB-crossing kinetics. In general, we observed a complete lack of correlation between these two sets of values for all time points (with correlation coefficient $R^2 < 0.1$; *SI Appendix*, Fig. S5 *B–D*), indicating that selective restriction of the barrier is protein-dependent, as opposed to concentration gradient-dependent.

Changes in Barrier Selectivity Following Neoangiogenic Tissue Repair. As stated previously, while we used one of the two eyes in the time course study, the other eye had been injured as a model of wound repair and pathological angiogenesis following laser treatments of corneal limbus. At 2 wk after surgery, whole-mount immunofluorescence images of the limbal vascular plexus showed an extensively distorted Schlemm's canal and the formation of a new vascular network comprising both blood and lymphatic vessels (Fig. 3*A*).

As noted earlier, a greater number of proteins entered the injured eye (Fig. 2). We asked whether this was due to the loss of barrier selectivity during neovascularization. Again, we assessed the relative abundance of ^{15}N-labeled proteins in serum to one another, as estimated by their NSAF indices. We then separated proteins into a group that cross the BAB in both uninjured and injured eyes and a group that cross only the injured barrier. Surprisingly, proteins in the second group had significantly lower levels of corresponding serum abundance compared with proteins in the first group (Fig. 3*B*), indicating possible selectivity as opposed to a simple concentration gradient that controls protein passage across the injured BAB. Indirect evidence in support of this assessment also lies within the proteins belonging to the first group that cross both injured and uninjured eyes; a greater number of these proteins showed reduced barrier crossing than showed increased crossing in the injured eye (32 vs. 9 in Fig. 3*C*), further suggesting that increased permeability caused by injury is associated with increased varieties of serum proteins entering aqueous.

Based on the speculation that even the BAB of the injured eye remains highly selective to protein passage, we next categorized these proteins by their function (Fig. 3*D*) to see whether specific functional groups are enriched following injury. Notably, categories associated with the immune complement system and immunity and with extracellular matrix proteins had a more prominent presence in the injured eyes (Fig. 3*D*, *Right*). This is consistent with the state of inflammation in tissue repair.

Inhibitory Complement Regulator Proteins Enter Aqueous in Tissue Repair. We were particularly interested in the large group of complement proteins and their regulatory factors with a greater number of proteins in the injured eye. We plotted their distribution patterns in blood and aqueous of each eye for up to 5 h following systemic injection of ^{15}N-labeled serum (Fig. 4*A* and *SI Appendix*, Fig. S6; a complete list of all 136 proteins is provided in *SI Appendix*, Fig. S3). With the sole exception of complement protein C3, which entered aqueous, there was undetectable entry of the majority of other complement proteins, such as C1 complex (including subunits C1q, C1s, C1ra, and C1rb), C4bpa, C7, C8, Ficolin/Fcn, and Mbl, regardless of the injury status of the eye (*SI Appendix*, Fig. S6). Meanwhile, a number of inhibitory complement regulators (CRegs), including complement factor H (Cfh) and factor H-related protein (Cfhr), factor B (Cfb), factor D (Cfd), factor I (Cfl), and vitronectin (Vtn), entered only the injured eye (Fig. 4*A*). It is likely that these CReg proteins (also termed regulators of complement activation or complement control proteins) are involved in the inflammation control necessary for tissue repair and vascular protection (25–27).

It is known that CReg proteins are also expressed locally by ocular tissues (14). To determine whether the observed entry of

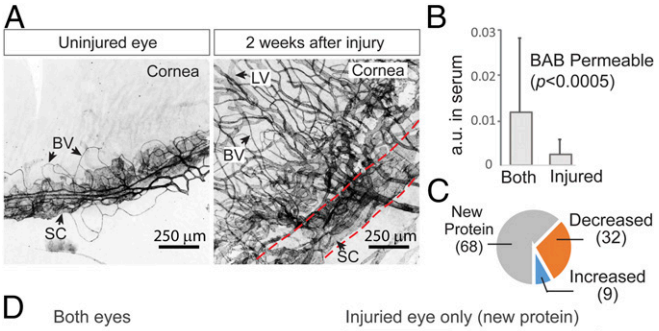

D

Both eyes		Injuried eye only (new protein)	
Peptidase inhibition	**Complement**	Peptidase inhibition	**Complement**
Serpina1a Serpina1b Serpina1c Serpina1d Serpina1e Serpina3c Serpina3f Serpina3g Serpina3m Serpina3n Serpinc1 Serpinf2	C3	Serpina10 Itih1 Itih2 Serpina6 Agt	C5 **Cfi** **Cfh** **Cfhr2** Cfd **Cfb** **Crp** **Vtn**
Coagulation	Plg Kng1	Metabolism	**Immunity-other**
Transport	Alb A1bg A2m Gc/Dbp Hbb-bs Hbb-b1Tf	Aldoa	A2m B2m H2-Q10 Lifr
Lipoprotein	Apoa1 Apoa4 Apoh	Redox	ECM and cell
Metabolism		Prdx2	Ecm1 Act Actb Actg1 Actc1 Actbl2 Fgb Tubb4b Azgp1 Afm Gsn Lrg Lum Fn1 Gpid1 Gpi
Hydrolase	ECM	Lipoprotein	
Pkm Tkt	Ahsg Cdh1	Apoa2	
Ces1c		Hydrolase	
Reduction-oxidation		Pon1 Ca2 Ica Clu	
Ceruloplasmin/Cp Gpx3		Coagulation	Transport
		F2 F12 Fga	Mug1 Hp Mug2 Rbp4 Tcn2

Fig. 3. Changes in aqueous barrier permeability following neovascularization and wound healing. (*A*) In the eye model, one of the two eyes was first injured with a laser and then allowed to recover for 2 wk. Whole-mount immunofluorescence staining of limbal vascular plexus (between dotted lines) using anti-CD31 showed destruction of Schlemm's canal (SC) and excessive neovascular growth of both blood vessels (BVs) and lymphatic vessels (LVs) in the recovering eye. (*B*) The abundance of individual serum proteins was measured by label-free quantification (*y*-axis). Those proteins with their ^{15}N-labeled species detected in aqueous were considered BAB- permeable. These proteins were divided into two groups: those detected in both eyes and those detected in only the injured eye. New proteins that crossed the BAB due to injury are those with lower serum abundance compared with proteins that were permitted to enter both eyes, including the normal eye. (*C*) When the amounts of those proteins appearing in both injured and uninjured eyes were compared (at 5 h; the colored pies), a greater number of proteins had decreased levels (32 proteins) than had increased levels (9 proteins). (*D*) Functional classification of proteins that crossed the uninjured barrier (*Left*) vs. proteins that entered only the injured eye (*Right*). Expansions of groups such as complement system and other immunities are evident (highlighted). Proteins known to be associated with age-related macular degeneration are in bold type.

CReg proteins from blood in the wound healing model correlates with elevated levels of these proteins in aqueous, we compared the MS label-free quantification indices in injured vs. uninjured eyes (*SI Appendix*, Fig. S7). Indeed, there was a general trend toward a more prominent presence of these proteins in the injured eyes.

Because the laser-induced angiogenesis model involved an initial injury of the corneal vascular plexus, we could not completely rule out nonspecific protein leak from the injured vessels instead of from the newly formed vessels. To avoid effects caused by direct vascular damage, we performed a different eye model by applying alkali burn to the avascular cornea (28). At 14 d after a unilateral alkali burn, corneal neovascular growth was evident, as shown by anti-CD31 staining of whole-mount specimens (Fig. 4*B*, *Left*). Aqueous humor was extracted from both eyes and then resolved by SDS/PAGE. Consistent with the proteomic results, immunoblotting of Cfh and Cfb showed very low baseline levels of these proteins in uninjured eyes compared with their levels in serum (Fig. 4*B*, *Right*). Importantly, in all three animals tested, there were markedly higher amounts of both Cfh and Cfb in the recovering eyes, likely attributable to distinct features of the new vessels' selective permeability.

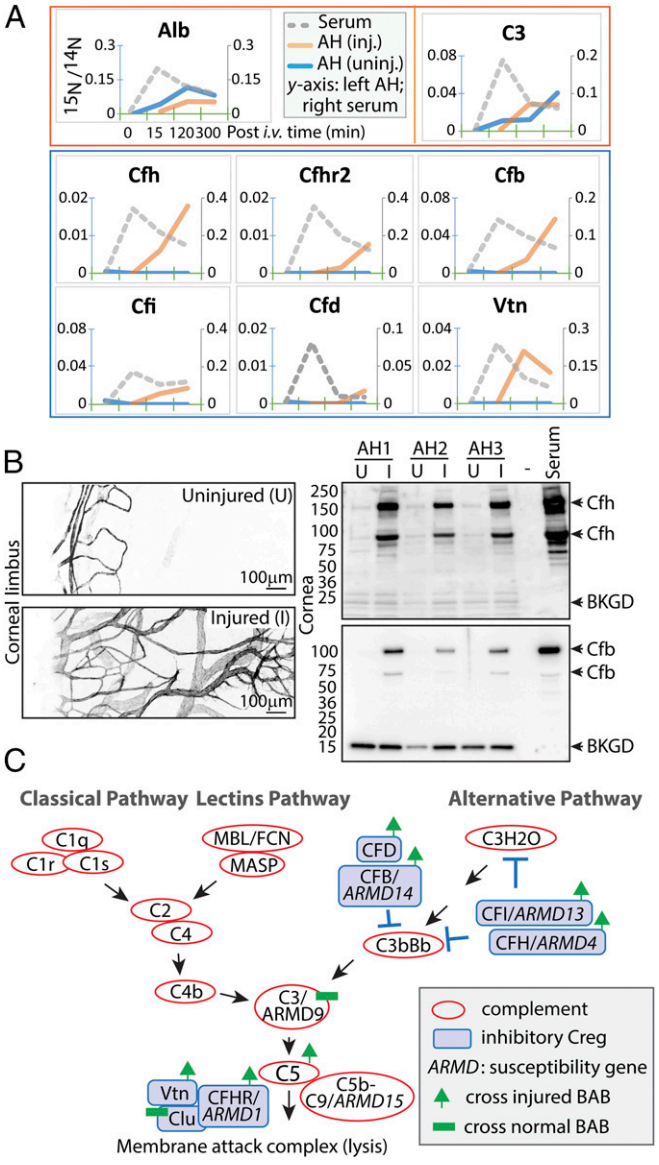

Fig. 4. Complement regulatory proteins enter aqueous in wound healing. (*A*) From the top, the red box shows representative proteins of albumin and C3 that entered the aqueous of both injured and uninjured eyes (legends shown for albumin; ^{15}N/^{14}N ratios: left scale for aqueous and right scale for serum), and the blue box contains proteins that entered the injured eyes but not the uninjured eyes. (*B*) Unilateral corneal treatment with alkali was applied to mice, and corneal neovascularization was evident 2 wk later (compare the anti-CD31 images of uninjured and injured eyes). Aqueous proteins were extracted from individual eyes in three mice (AH1–3). Immunoblotting shows levels of Cfh and Cfb proteins. (*C*) The complement pathways in association with AMD. Red circles represent complement-activating proteins; blue boxes, complement regulatory proteins. Proteins associated with genetic susceptibility to AMD are annotated (*ARMD1–15*), and proteins with increased permeability in wound healing and proteins with constant barrier-crossing kinetics are indicated.

Discussion

Selective restriction of protein passage across specialized vascular barriers, such as the blood-placental, blood-brain, blood-testis, and glomerular filtration barriers, among others, are of great interest in vascular biology and clinical medicine. In developing the ^{15}N isotope tracing methodology, we chose the ocular model described herein for the following reasons: (*i*) aqueous humor can be accessed easily and cleanly; (*ii*) barrier abnormalities generally reflect poor overall vascular health and disease states; (*iii*) the ability to conduct unilateral treatment is suitable for comparative studies of disease vs. health conditions; (*iv*) certain eye diseases are associated with neovascularization and leakage of the barriers, and thus our analytical tool may expand clinical options; and (*v*) knowledge of characteristics of blood barriers is needed to enhance drug delivery. The SILAM-based approach identified a large number of plasma proteins that selectively enter aqueous, including the serpin family peptidases, complement C3, apolipoproteins, and the transport carrier proteins that are the main constituents of aqueous proteins, among others.

Homeostatic regulation of the aqueous humor is important for normal eye function, including maintaining ocular immune privilege (29). The various permselective blood barriers in the eye are essential to restrict plasma protein entry, but the mechanisms underlying this selectivity are incompletely understood (2). Instead of using single molecular tracers, our approach labels all proteins in serum with ^{15}N atoms, so that individual ^{15}N-containing proteins that enter aqueous from blood circulation can be individually identified and measured by MS. This methodology effectively avoids ambiguities in distinguishing serum-derived proteins from those expressed by eye tissues.

Plasma proteins cross the biological barriers by several different mechanisms. In the blood-brain barrier (BBB), chemical drugs and proteins cross the barrier via receptor- or adsorptive-mediated transcytosis, which enables high selectivity (30, 31). In other barriers, such as the glomerular filtration barrier of the kidney, the permeability of plasma proteins is restricted by size and charge selectivity (32). The selectivity of these barriers to serum proteins can be altered by the disruption of barrier structure in pathological conditions; for example, breakdown of the BBB leads to leakages and perivascular accumulation of blood-derived fibrinogen, thrombin, albumin, IgG, and hemosiderin deposits (33). Our results show disparities in aqueous permeability among serum proteins without apparent size and charge preferences (*SI Appendix*, Figs. S3 and S8), suggesting a protein-dependent selectivity of the BAB resembling that of the BBB. Following ocular wound healing and associated neovascularization, there was an increase in the variety of serum proteins in the aqueous, with enrichment of proteins of certain functional categories (Fig. 3). This observation suggests that the neovascular vessels still have selectivity distinct from the originally formed vessels in the eye. In human neovascular glaucoma (NVG), which is caused by a precondition of neovascularization of the iris (NVI, also known as rubeosis iridis), a change in vascular permeability is believed to have a key role in pathogenesis (34).

Notably, there was an increase in CRegs entering the injured eye, including members of complement factor families Cfh, Cfhr2, Cfb, Cfd, Cfi, and Vtn. These complement inhibitors, with the exception of Cfb, were detected only in the injured eyes and not in healthy aqueous. In contrast to these inhibitory CRegs, activators of the complement system, with the exception of C3, remained in serum and did not enter aqueous. These include members of C1, C4, C7, C8, Fcn, and Mbl family proteins that remained restricted to plasma and were never found in aqueous (*SI Appendix*, Fig. S6). It is possible that inhibitory CRegs play an important role during tissue repair in the eye, limiting complement-mediated vascular injury. Intriguingly, several of these CRegs are encoded by genes associated with age-related macular degeneration (AMD) (35, 36); for example, AMD susceptibility allele *ARMD1* encodes Cfhr1/3 (37), *ARMD4* encodes Cfh (38–41), *ARMD13* encodes Cfi (35), and *ARMD14* encodes Cfb (42) (Fig. 4*C*). In addition, Vtn of the terminal membrane attack complex is a constituent of ocular drusen in AMD (43). AMD is a progressive retinal disease associated with pathological neovascularization and leakage of plasma proteins through a compromised BRB (44). Although the BRB and the BAB are different barriers, they share structural similarities, and there is an evolving concept that these two barriers work cooperatively (2). Although the proteomic observations in the present study were not from an AMD model, it is plausible that enhanced entry of these CRegs across the choriocapillary/blood barrier is similarly needed to protect the choroid from inflammation and injury. The aqueous model suggests that selective transfer of CRegs from the plasma occurs during injury and likely promotes physiological wound repair that involves neovascularization. Certain risk alleles of these proteins associated with AMD are believed to result in compromised CReg functions (e.g., loss of function, decreased expression), and therefore lead to excessive inflammatory reactions causing vascular leak. Our results raise the possibility that additional mechanisms, including altered or defective transport of CReg proteins, may play a role in the development and progression of eye diseases and healing.

The ability to label whole serum was critical in our study for measurement of protein passage. This method has some limitations, however. First, SILAM-based semiquantification measures the relative amounts between ^{15}N- and ^{14}N-containing proteins, and thus the $^{15}N/^{14}N$ ratios are also influenced by the steady-state amounts of individual ^{14}N-containing proteins, each of which possibly differs between normal and injured eyes. In addition, although SILAM-labeled tracers resemble their endogenous counterparts without the need for chemical treatment, there is a substantial cost associated with raising these metabolically labeled animals using isotopes. This precluded us from including more replicates and time points. Due to the excessive cost of labeling whole organisms, SILAM has only been practiced on small animals, such as rodents (16), in addition to nonmammal species of worm, fruit fly, and yeast (45). Another difficulty is the limited amount of aqueous that can be collected from a mouse eye, which affected the proteomic coverage of low-abundant proteins and also precluded us from performing aqueous extractions in a longitudinal series all from one eye as are normally performed in larger animals such as rabbit and cat. Instead, our time series studies required the use of multiple mice, each representing a single time point. Therefore, experimental variability among these mice for individual time points will contribute to a certain degree of inaccuracy in calculating kinetic curves.

In summary, we present a semiquantitative strategy using ^{15}N-labeled whole serum to study the passage of proteins from blood to aqueous humor. Our results provide proteome-level insight into the selectivity of the BAB. By directly comparing normal and injured eyes, we observed significantly enhanced permeability to complement regulatory proteins associated with neovascularization.

Materials and Methods

Additional information is provided in *SI Appendix, Materials and Methods*.

Metabolic ^{15}N Labeling of Serum Donor Mice. Northwestern University's Institutional Animal Care and Use Committee approved all animal procedures (approved protocols IS00000429 and IS00000862). Gamma irradiation-sterilized ^{15}N-enriched spirulina algae was used to prepare rodent chow as described previously (22). Ten C57BL/6J female mice (The Jackson Laboratory) were metabolically labeled with a ^{15}N-rich spirulina-based diet (Cambridge Isotopes and Harlan Laboratories) for 12 wk starting at postnatal day 21 (16). The ^{15}N protein enrichment in brain was determined to be approximately 90–95%. Blood from the mice was harvested by cervical dislocation, followed by decapitation bleeding. Once blood clots formed, serum was collected and stored at −80 °C until use.

Aqueous Collection and Proteomic Sample Preparation. The female C57BL/6J mice were raised on a regular ^{14}N diet. The mice were housed under conventional conditions with free access to regular chow and nonacidified water (via an automated watering system) and with a 12:12-h light/dark cycle. Each mouse received a single 300-μL dose of ^{15}N-serum via a tail vein injection. Each mouse was assigned to a single time point. The blood sample for serum collection at that time point was from tail bleeding (approximately 20 μL) immediately before aqueous collection. Following cervical dislocation, aqueous was collected using a Hamilton syringe equipped with a Hamilton 32-gauge needle. Up to 5 μL of aqueous was collected from each eye. Both serum (5 μL) and aqueous samples were then subjected to standard denaturing (by 6 M urea), reduction, and alkylation (10 mM DTT and 30 mM iodoacetamide), followed by digestion with trypsin and LysC (Promega). The resulting tryptic peptides were recovered using C18 columns (Thermo Fisher Scientific) following the manufacturer's standard protocol.

Data Analysis and Statistics. Out of a total of 1,240 proteins in aqueous and 842 proteins in serum identified by MS at 15 min (*SI Appendix*, Fig. S2), we considered only 517 of the 842 serum proteins that have their corresponding ^{15}N components. We then combined protein isoforms based on Uniprot GeneIDs and kept a nonredundant set of 136 genes/proteins (*SI Appendix*, Fig. S2) on our final list, then and calculated their blood-to-aqueous redistribution kinetics. The quantification values of $^{14}N/^{15}N$ ratios, NSAF, and emPAI for all 1,558 proteins (based on distinct accession numbers) across all time points were populated in a master spreadsheet (Dataset S1). The R^2 values for correlation coefficients were calculated using Excel (*SI Appendix*, Fig. S4). In the comparison between proteins found in both eyes and those found only in injured eyes shown in Fig. 3*B*, a standard two-tailed *t* test was used to derive the *P* values.

Proteomics Data Availability. All raw spectrum data are available through the MassIVE database (https://massive.ucsd.edu/ProteoSAFe/static/massive.jsp) via ProteomeXchange identifier PXD010366.

ACKNOWLEDGMENTS. This work was supported by the National Institutes of Health (Grants R01 EY026286, to X.L.; R00 DC013805, to J.N.S.; and R01 EY025799, to S.E.Q.). We thank Qunfeng Dong (Loyola University) for advice on statistics and George Anagnos for assistance with data analysis. We also thank the Center for Advanced Microscopy for imaging services and the Center for Comparative Medicine of Northwestern University for animal care.

1. Cunha-Vaz J, Bernardes R, Lobo C (2011) Blood-retinal barrier. *Eur J Ophthalmol* 21(Suppl 6):S3–S9.
2. Freddo TF (2013) A contemporary concept of the blood-aqueous barrier. *Prog Retin Eye Res* 32:181–195.
3. Butler JM, Unger WG, Grierson I (1988) Recent experimental studies on the blood-aqueous barrier: The anatomical basis of the response to injury. *Eye (Lond)* 2(Suppl): S213–S220.
4. Cunha-Vaz J (2017) Mechanisms of retinal fluid accumulation and blood-retinal barrier breakdown. *Dev Ophthalmol* 58:11–20.
5. Stein-Streilein J, Streilein JW (2002) Anterior chamber-associated immune deviation (ACAID): Regulation, biological relevance, and implications for therapy. *Int Rev Immunol* 21:123–152.
6. Freddo TF, Bartels SP, Barsotti MF, Kamm RD (1990) The source of proteins in the aqueous humor of the normal rabbit. *Invest Ophthalmol Vis Sci* 31:125–137.
7. Johnson M, Gong H, Freddo TF, Ritter N, Kamm R (1993) Serum proteins and aqueous outflow resistance in bovine eyes. *Invest Ophthalmol Vis Sci* 34:3549–3557.
8. McLaren JW (2009) Measurement of aqueous humor flow. *Exp Eye Res* 88:641–647.
9. Green K, et al. (1977) Fate of anterior chamber tracers in the living rhesus monkey eye with evidence for uveo-vortex outflow. *Trans Ophthalmol Soc U K* 97:731–739.
10. Raviola G, Butler JM (1983) Unidirectional vesicular transport mechanism in retinal vessels. *Invest Ophthalmol Vis Sci* 24:1465–1474.
11. Kodama T, Reddy VN, Macri FJ (1983) The arterially perfused enucleated rabbit eye as a model for studying aqueous humor formation. *Ophthalmic Res* 15:225–233.
12. Bert RJ, et al. (2006) Demonstration of an anterior diffusional pathway for solutes in the normal human eye with high spatial resolution contrast-enhanced dynamic MR imaging. *Invest Ophthalmol Vis Sci* 47:5153–5162.
13. Chowdhury UR, Madden BJ, Charlesworth MC, Fautsch MP (2010) Proteome analysis of human aqueous humor. *Invest Ophthalmol Vis Sci* 51:4921–4931.
14. Keir LS, et al. (2017) VEGF regulates local inhibitory complement proteins in the eye and kidney. *J Clin Invest* 127:199–214.
15. Murthy KR, et al. (2015) Proteomics of human aqueous humor. *OMICS* 19:283–293.
16. Wu CC, MacCoss MJ, Howell KE, Matthews DE, Yates JR, 3rd (2004) Metabolic labeling of mammalian organisms with stable isotopes for quantitative proteomic analysis. *Anal Chem* 76:4951–4959.
17. Gouw JW, Tops BB, Krijgsveld J (2011) Metabolic labeling of model organisms using heavy nitrogen (15N). *Methods Mol Biol* 753:29–42.
18. McClatchy DB, Yates JR, 3rd (2008) Stable isotope labeling of mammals (SILAM). *CSH Protoc* 2008:pdb.prot4940.
19. Florens L, et al. (2006) Analyzing chromatin remodeling complexes using shotgun proteomics and normalized spectral abundance factors. *Methods* 40:303–311.
20. Ishihama Y, et al. (2005) Exponentially modified protein abundance index (emPAI) for estimation of absolute protein amount in proteomics by the number of sequenced peptides per protein. *Mol Cell Proteomics* 4:1265–1272.
21. Slingsby C, Wistow GJ, Clark AR (2013) Evolution of crystallins for a role in the vertebrate eye lens. *Protein Sci* 22:367–380.
22. Tomarev SI, Piatigorsky J (1996) Lens crystallins of invertebrates: Diversity and recruitment from detoxification enzymes and novel proteins. *Eur J Biochem* 235: 449–465.
23. Wojcik KA, Kaminska A, Blasiak J, Szaflik J, Szaflik JP (2013) Oxidative stress in the pathogenesis of keratoconus and Fuchs endothelial corneal dystrophy. *Int J Mol Sci* 14:19294–19308.
24. Gerashchenko DY, et al. (1998) Localization of lipocalin-type prostaglandin D synthase (beta-trace) in iris, ciliary body, and eye fluids. *Invest Ophthalmol Vis Sci* 39:198–203.
25. Ferluga J, Kouser L, Murugaiah V, Sim RB, Kishore U (2017) Potential influences of complement factor H in autoimmune inflammatory and thrombotic disorders. *Mol Immunol* 84:84–106.
26. Fischetti F, Tedesco F (2006) Cross-talk between the complement system and endothelial cells in physiologic conditions and in vascular diseases. *Autoimmunity* 39: 417–428.
27. Kather JN, Kroll J (2014) Transgenic mouse models of corneal neovascularization: New perspectives for angiogenesis research. *Invest Ophthalmol Vis Sci* 55:7637–7651.
28. Kubota M, et al. (2011) Hydrogen and N-acetyl-L-cysteine rescue oxidative stress-induced angiogenesis in a mouse corneal alkali-burn model. *Invest Ophthalmol Vis Sci* 52:427–433.
29. de Andrade FA, et al. (2016) The autoimmune diseases of the eyes. *Autoimmun Rev* 15:258–271.
30. Rubin LL, Staddon JM (1999) The cell biology of the blood-brain barrier. *Annu Rev Neurosci* 22:11–28.
31. Poduslo JF, Curran GL, Berg CT (1994) Macromolecular permeability across the blood-nerve and blood-brain barriers. *Proc Natl Acad Sci USA* 91:5705–5709.
32. Scott RP, Quaggin SE (2015) Review series: The cell biology of renal filtration. *J Cell Biol* 209:199–210.
33. Montagne A, Zhao Z, Zlokovic BV (2017) Alzheimer's disease: A matter of blood-brain barrier dysfunction? *J Exp Med* 214:3151–3169.
34. Rodrigues GB, et al. (2016) Neovascular glaucoma: A review. *Int J Retina Vitreous* 2:26.
35. Dryja TP (2016) Early insight into neovascular age-related macular degeneration. *JAMA Ophthalmol* 134:1281–1282.
36. Fritsche LG, et al. (2016) A large genome-wide association study of age-related macular degeneration highlights contributions of rare and common variants. *Nat Genet* 48:134–143.
37. Hughes AE, et al. (2006) A common CFH haplotype, with deletion of CFHR1 and CFHR3, is associated with lower risk of age-related macular degeneration. *Nat Genet* 38:1173–1177.
38. Klein RJ, et al. (2005) Complement factor H polymorphism in age-related macular degeneration. *Science* 308:385–389.
39. Edwards AO, et al. (2005) Complement factor H polymorphism and age-related macular degeneration. *Science* 308:421–424.
40. Haines JL, et al. (2005) Complement factor H variant increases the risk of age-related macular degeneration. *Science* 308:419–421.
41. Mattapallil MJ, Caspi RR (2017) Compliments of factor H: What's in it for AMD? *Immunity* 46:167–169.
42. Gold B, et al.; AMD Genetics Clinical Study Group (2006) Variation in factor B (BF) and complement component 2 (C2) genes is associated with age-related macular degeneration. *Nat Genet* 38:458–462.
43. Crabb JW, et al. (2002) Drusen proteome analysis: An approach to the etiology of age-related macular degeneration. *Proc Natl Acad Sci USA* 99:14682–14687.
44. Cunha-Vaz JG (2004) The blood-retinal barriers system: Basic concepts and clinical evaluation. *Exp Eye Res* 78:715–721.
45. Krijgsveld J, et al. (2003) Metabolic labeling of *C. elegans* and *D. melanogaster* for quantitative proteomics. *Nat Biotechnol* 21:927–931.